Citation: Yi Tian, Ruijia Liu, Wei Wang, et al. Modified equivalent plane-strain model on consolidation of soft ground improved by preloading with PVDs. *Journal of Harbin Institute of Technology (New Series)*. DOI: 10.11916/j.issn.1005-9113.2025136

Modified Equivalent Plane-Strain Model on Consolidation of Soft Ground Improved by Preloading with PVDs

Yi Tian[1,2], *Ruijia Liu*[1], *Wei Wang*[3], *Hui Long*[1], *Wenbing Wu*[4] *and Yue Gui*[4] *

(*1. Department of Civil Engineering, Faculty of Civil Engineering and Mechanics, Kunming University of Science and Technology, Kunming 650500, China;*
2. Kunming Prospecting Design Institute of China Nonferrous Metals Industry Co., Ltd., Kunming 650051, China;
3. China Electronics Digital (Shanghai) Technology Co., Ltd., Shanghai 201800, China;
4. Faculty of Engineering, China University of Geosciences, Wuhan 430074, China)

Abstract: The combination of vacuum preloading and Prefabricated Vertical Drains (PVDs) has been widely used in coastal engineering projects to improve large-scale soft ground. Nevertheless, more precise theoretical models are still desperately needed to meet the increasingly stringent deformation design specifications. To refine the numerical simulation of the soft ground improved by PVDs, a modified plane-strain equivalent model is proposed by incorporating the shape effect of PVDs based on the permeability matching method. The model is then validated through comparisons with a single-drain analytical model, a realistic 3D finite element model, and measured data from a field case history. The case analysis indicates that the surrounding soil adjacent to the treated zone is also influenced by vacuum pressure and predominantly exhibits lateral displacement during preloading. The lateral displacement in the surrounding soil without PVDs decreases with depth, with the maximum value at the soil surface occurring near the edges of the treated zone. The parametric analyses suggest that, under identical total load magnitudes, reducing the surcharge load and/or the loading rate can effectively decrease outward displacements of the surrounding soil. In practical ground improvement, the implementation of an optimal combined vacuum and surcharge preloading is shown to be effective in mitigating the adverse impacts of lateral displacements on adjacent environments.

Keywords: consolidation; PVDs; plane-strain model; vacuum preloading; lateral deformation
CLC number: TU4 **Document code**: A **Article ID**: 1005-9113(2026)00-0000-13

0 Introduction

The rapid urbanization and infrastructure development in coastal regions have intensified the demand for constructing large-scale engineering projects, such as ports, highways, and land reclamation facilities, on soft clay deposits. However, these geologically challenging soils, characterized by high compressibility, low permeability, and prolonged consolidation behavior, pose significant risks to structural stability and long-term performance[1-7]. The combined application of vacuum preloading and Prefabricated Vertical Drains (PVDs) has emerged as an essential solution to accelerate consolidation and enhance soil strength and has been widely used in coastal ground treatment projects[8-15], therefore, increasingly stringent design requirements of modern coastal engineering urgently demand a robust theoretical model to predict the consolidation response of the ground.

The engineering design of PVDs - enhanced ground systems predominantly relies on consolidation theory. Since the seminal work of Reginald et al.[16] established the radial consolidation theory for sand drain-improved foundations under surcharge loading, substantial research has been dedicated to advancing consolidation models for PVD applications[17-19]. A

Received 2025-11-07.
This work was sponsored by National Natural Science Foundation of China (Grant No. 52468052, 52408367), Yunnan Fundamental Research Projects (Grant No. 202401CF070127).
* Corresponding author: Yue Gui, Ph.D, Professor. Email: gydrgui@kmust.edu.cn.

fundamental challenge arises from the geometric disparity between conventional cylindrical sand drains and modern band-shaped PVDs[20], which motivated Hansbo et al.[21] to pioneer a perimeter-based equivalence method. This approach converts PVD cross-sections into equivalent cylindrical forms while incorporating well resistance and smear effects into modified consolidation equations that remain prevalent in contemporary practice. Subsequent studies have proposed alternative equivalence criteria for radius conversion of PVDs[22-25], yet persistent discrepancies persist regarding optimal methodology selection for field applications. The geometric mismatch between banded PVD and cylindrical sand drain stems from their distinct seepage field configurations.

In contrast to the circular seepage equipotential surrounding a sand drain, the pronounced width-to-thickness ratio of PVDs generates elliptical seepage equipotential, a feature known as the shape effect of PVDs. To account for this, Huang et al.[26] formulated an elliptical cylinder equivalence hypothesis, later refined by Tian et al.[27] into their Elliptical Cylindrical Equivalent Model (ECEM). Based on the ECEM, refined consolidation models have been developed for PVD-improved ground by considering nonlinear compressibility and permeability of soil [28], unsaturated soil [29], and large-strain characteristic of soil [30]. The aforementioned consolidation models predominantly employ single-drain analysis as their representative unit, rendering them suitable for predicting soil consolidation behavior under uniformly distributed loads. However, in practical engineering scenarios, ground treatment zones typically involve a large drain group consisting thousands of PVDs. Furthermore, the soils near the treated zone exhibit significant lateral deformation [31] that cannot be adequately captured by the single-drain models. Therefore, the development of a drain-group model is required to simulate the deformation behaviors throughout whole treatment regions.

In the finite element numerical simulation, a realistic 3D model for the drain-group system usually requires numerous meshes due to the large number of PVDs and their tiny cross-sectional size compared to the entire treatment area. This seriously affects the computational efficiency. Thus, the equivalent treatment of the calculation model is imperative for the drain-group consolidation analysis. Accordingly, Hird et al.[32-33] pioneered a plane-strain equivalent method to simplify the complex drain-group model into plane-strain configurations. With this method, the PVDs in the drain-group system are represented with drained walls, which can greatly improve computational efficiency of the finite element model.

Two primary equivalence approaches, permeability matching method and geometric matching method, are commonly implemented in the plane-strain equivalent model. The former maintains constant PVD spacing while adjusting the permeability coefficient of soils to preserve consolidation equivalence. The latter preserves the permeability coefficient while optimizing the drain spacing to achieve consolidation equivalence. Indraratna et al. [34] extended the permeability matching method by incorporating smear zone effects induced by PVDs installation (i.e., divided the influence zone of each PVD into disturbed zone and undisturbed zone). Although such separate equivalence treatment for disturbed and undisturbed zones can slightly improve the calculation accuracy, it inevitably increases model complexity. Therefore, the original permeability matching method proposed by Hird et al.[33] remains predominant in contemporary practice. However, it was derived based on the conventional equivalent cylindrical model and failed to account for the aforementioned shape effect of PVDs.

Building upon the ECEM framework, this study establishes a modified equivalent plane-strain model through implementation of the permeability matching method. Utilizing the derived equivalent permeability coefficient, a numerical model for PVDs-improved ground is developed using COMSOL Multiphysics, with subsequent validation against existing engineering case studies. Based on the numerical model, a systematic investigation into lateral deformation characteristics of PVDs-improved ground systems is conducted.

1 Modified Equivalent plane-strain Model Based on ECEM

According to the plane-strain equivalent methodology proposed by Hird et al.[32], each PVD is converted to a drained wall to achieve efficient numerical calculation of the drain-group system. The equivalent horizontal permeability coefficient of soil, the widths of equivalent drained wall and equivalent single-drain influence zone need to be determined

before numerical modelling. In order to consider the shape effect of PVDs, the ECEM proposed by Tian et al.[8] is suitable as the original model of the plane-strain equivalence. The ECEM is formulated in an elliptical cylindrical coordinate system, for which the corresponding consolidation equations and solutions have been thoroughly derived by Tian et al.[28].

Fig. 1 presents the single-drain unit of the ECEM and the equivalent plane-strain unit, where ρ_w, ρ_s, ρ_e denote the horizontal coordinates of the outer boundaries of PVDs, smear zone, and single-drain influence zone in the ECEM, respectively. L is the thickness of improved soil, b_w and B are the half widths of equivalent drained wall and equivalent single-drain influence zone, respectively. A surcharge load, q, is uniformly applied on the soil surface. Meanwhile, a vacuum load, $-p_v$, is applied from PVDs top. In order to perform equivalent conversion, the consolidation degree is derived for the equivalent plane-strain model as follows.

In order to achieve theoretical modeling, basic assumptions are made as follows:

(1) The equal vertical strain hypothesis[16] is adopted.

(2) The water flow in the soil is governed by Darcy's law.

(3) The soil is fully saturated, and solid grains and pore water within the soil are incompressible.

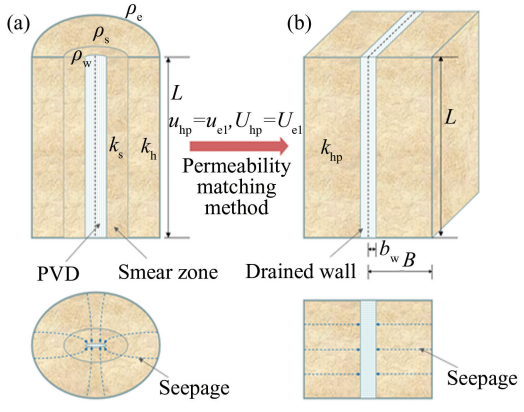

Fig. 1 plane-strain equivalent methodology: (a) ECEM, (b) equivalent plane-strain model

In the plane-strain model shown in Fig. 1(b), according to the principle of flow continuity and Darcy's law for flow in the soil, the following equation can be obtained[34]:

$$\frac{\partial u_{hp}}{\partial x}=\frac{\gamma_w}{k_{hp}}(B-x)\frac{\partial \varepsilon_v}{\partial t} \tag{1}$$

where u_{hp} is excess pore water pressure induced by horizontal drainage in equivalent plane-strain model, γ_w is unit weight of water, ε_v is the average volumetric strain of the soil mass, k_{hp} is horizontal permeability coefficient in equivalent plane-strain model, B is the half width of equivalent single-drain influence zone, x is the horizontal coordinate from the centerline of the equivalent drained wall, t is consolidation time, and the symbol ∂ indicates a partial derivative. At the PVD – soil boundary ($x=b_w$), the flow continuity yields the following equation:

$$2k_{hp}\left(\frac{\partial u_{hp}}{\partial x}\right)_{x=b_w}=-q_w\frac{\partial^2 u_w}{\partial z^2} \tag{2}$$

where q_w is discharge capacity of PVD under unit hydraulic gradient, u_w is excess pore water pressure in PVD, b_w is the half width of equivalent drained wall, z is the vertical coordinate measured downward from the ground surface.

The boundary conditions can be expressed as follows:

$$u_w|_{z=0}=-p_v \tag{3}$$

$$\left.\frac{\partial u_w}{\partial z}\right|_{z=L}=0 \tag{4}$$

$$\left.\frac{\partial u_{hp}}{\partial x}\right|_{x=B}=0 \tag{5}$$

Under the above boundary conditions, substitution of Eq. (1) into Eq. (2) gives:

$$u_w=2\frac{\gamma_w}{q_w}(B-b_w)\left(Lz-\frac{1}{2}z^2\right)\frac{\partial \varepsilon_v}{\partial t}-p_v \tag{6}$$

Integrating Eq. (1) under the continuity condition (Eq. (2) and the boundary condition (Eq. (3) and (4)) yields:

$$u_{hp}=\frac{\gamma_w}{k_{hp}}\left[\left(Bx-\frac{1}{2}x^2\right)-\left(Bb_w-\frac{1}{2}b_w^2\right)\right]\frac{\partial \varepsilon_v}{\partial t}+2\frac{\gamma_w}{q_w}(B-b_w)\left(Lz-\frac{1}{2}z^2\right)\frac{\partial \varepsilon_v}{\partial t}-p_v \tag{7}$$

The average excess pore water pressure on a horizontal plane with depth, z, can be expressed as follow:

$$\bar{u}_{hp}=\frac{\int_{b_w}^{B}u_{hp}dx}{B-b_w} \tag{8}$$

Substituting Eq. (7) into Eq. (8) yields:

$$\bar{u}_{hp}=\frac{B^2\gamma_w\mu_{hp}}{2k_{hp}}\frac{\partial \varepsilon_v}{\partial t}-p_v \tag{9}$$

where,

$$\mu_{hp} = F_{hp} + \frac{2\,k_{hp}}{B^2\,q_w}(B - b_w)\,(2Lz - z^2) \tag{10}$$

$$F_{hp} = \frac{2}{3} + \frac{2}{3}\frac{b_w}{B} - \frac{1}{3}\frac{b_w^2}{B^2} - 2\,\frac{b_w}{B} + \frac{b_w^2}{B^2} \tag{11}$$

When considering instantaneous loads uniformly applied on the soil top, the principle of effective stress can be written as follow[34]:

$$\frac{\partial\,\varepsilon_v}{\partial t} = -\,m_v\,\frac{\partial\,\bar{u}_{hp}}{\partial t} \tag{12}$$

where, m_v is coefficient of volumetric compression.

Substituting Eq. (12) into Eq. (9) yields:

$$\frac{\partial\,\bar{u}_{hp}}{\partial t} + \frac{2\,C_{hp}}{\mu_{hp}\,B^2}\bar{u} + \frac{2\,C_{hp}}{\mu_{hp}\,B^2}\,p_v = 0 \tag{13}$$

where, C_{hp} is the coefficient of consolidation in the equivalent plane-strain model, defined as $C_{hp} = \dfrac{k_{hp}}{\gamma_w\,m_v}$.

Solving Eq. (13) yields:

$$\bar{u}_{hp} = (u_0 + p_v)\,exp\left(-\frac{2\,C_{hp}}{\mu_{hp}\,B^2}t\right) - p_v \tag{14}$$

where, u_0 is initial excess pore water pressure due to the initial surcharge load.

The average consolidation degree of soil in a plane-strain model can be derived as follows:

$$U_{hp} = 1 - \frac{\bar{u}_{hp}}{u_0} = 1 - exp\left(-\frac{8}{\mu_{el}}\,T_{hp}\right) \tag{15}$$

where, T_{hp} is the time factor of the equivalent plane-strain model, defined as $T_{hp} = \dfrac{C_{hp}}{4\,B^2}t$, μ_{el} is the well resistance parameter in the ECEM.

When considering only horizontal drainage in soil, the average excess pore water pressure in the ECEM can be expressed as[30]:

$$\bar{u}_{el} = (u_0 + p_v)\,exp\left(-\frac{8\,T_{el}}{\mu_{el}}\right) - p_v \tag{16}$$

where, T_{el} is the time factor of the ECEM.

The corresponding average consolidation degree can be expressed as:

$$U_{el} = 1 - exp\left(-\frac{8}{\mu_{el}}\,T_h\right) \tag{17}$$

in which,

$$\mu_{el} = F_{el} + \frac{2\,k_h}{R_e^2\,q_w}\pi\,R_d^2(A_e - A_d)\left(Lz - \frac{1}{2}z^2\right) \tag{18}$$

where, $T_h = \dfrac{C_h t}{4\,R_e^2}$, $C_h = \dfrac{k_h}{\gamma_w\,m_v}$, $F_{el} = \dfrac{F_{el1} + F_{el2}}{\rho_e^2(A_e - A_d)}$. T_h is horizontal consolidation time factor, R_e is the equivalent radius of the influence zone, R_d is the equivalent radius of the PVD, A_e is the area parameter corresponding to the influence zone in the elliptical cylindrical coordinate system, A_d is the area parameter corresponding to the PVD in the elliptical cylindrical coordinate system, ρ_e is the horizontal coordinate of the outer boundary of the influence zone, F_{el} is an auxiliary function in the ECEM, defined by the auxiliary functions F_{el1} and F_{el2}.

in which,

$$F_{el1} = \kappa\left[(A_e^2 - 2\,M_d^2)\,ln\,s_{el} - (B_s - B_d)\,A_e + \frac{1}{4}(A_s\,B_s - A_d\,B_d)\right] \tag{19}$$

where, κ is index of soil expansion, M_d is a geometric parameter associated with the PVD cross-section in the ECEM, s_{el} is smear zone ratio in the ECEM, A_s is the area parameter corresponding to the smear zone in the elliptical cylindrical coordinate system, B_e, B_s, and B_d are the corresponding geometric parameters of the influence zone, smear zone, and PVD, respectively.

$$F_{el2} = (A_e^2 - 2\,M_d^2)\,ln\frac{n_{el}}{s_{el}} - (B_e - B_s)\,A_e + \frac{1}{4}(A_e\,B_e - A_s\,B_s) \tag{20}$$

where, n_{el} is influence zone ratio in the ECEM.

$$M_d = \frac{a_d - b_d}{a_d + b_d} \tag{21}$$

where, $A_d = \rho_d^2 - \dfrac{M_d^2}{\rho_d^2}$, $B_d = \rho_d^2 + \dfrac{M_d^2}{\rho_d^2}$, $A_e = \rho_e^2 - \dfrac{M_d^2}{\rho_e^2}$, $B_e = \rho_e^2 + \dfrac{M_d^2}{\rho_e^2}$, $A_s = \rho_s^2 - \dfrac{M_d^2}{\rho_s^2}$, $B_s = \rho_s^2 + \dfrac{M_d^2}{\rho_s^2}$, $s_{el} = \dfrac{\rho_s}{\rho_d}$, $n_{el} = \dfrac{\rho_e}{\rho_d}$.

Under the equivalent condition that $\bar{u}_{hp} = \bar{u}_{el}$ and $U_{hp} = U_{el}$ for any time, performing equivalent conversion between ECEM and plane-strain model yields:

$$\frac{T_{hp}}{\mu_{hp}} = \frac{T_h}{\mu_{el}} \tag{22}$$

Substituting Eq. (10) and (18) into Eq. (22), the equivalent coefficient of permeability in the plane-strain model can be obtained as follows:

$$k_{hp} = \frac{F_{hp}}{F_{el} + \left[\dfrac{1}{R_e^2}\pi\,R_d^2(A_e - A_d) - \dfrac{2}{R_e^2}(B - b_w)\right]\dfrac{k_h}{q_w}(2Lz - z^2)}.$$

$$\frac{B^2}{R_e^2} k_h \tag{23}$$

Accordingly, the equivalent coefficient of permeability for the plane-strain model is determined by substituting known horizontal permeability coefficient of soil (k_h), the half width of equivalent drained wall (b_w), and the half width of equivalent single-drain influence zone (B), into Eq. (23). For computational convenience, b_w is taken as half of the actual PVD thickness, and B is set equal to half of the PVD spacing, namely, $b_w = \delta/2$ and $B = d/2$. Such equivalent method is referred to as the modified permeability matching method incorporating the shape effect of PVDs. The equivalent horizontal permeability coefficient calculated from Eq. (23) is incorporated into the plane-strain model (shown in Fig. 1(b)), yielding corresponding modified equivalent plane-strain model.

In the numerical simulation of drain-group systems, each unit cell of single-PVD influence zone is represented by the modified equivalent plane-strain model, where the soil's horizontal permeability is assigned the equivalent permeability coefficient derived from Eq. (23), while the vertical permeability coefficient retains its actual measured value without equivalent transformation. Through performing such equivalent transformation, the complex 3D consolidation problem of drain-group systems is equivalent to a simple 2D model, which will significantly enhance computational efficiency. The overall computational workflow of the modified equivalent plane-strain model is illustrated in Fig. 2.

2 Comparative Validation

In order to rigorously verify the rationality of the modified equivalent plane-strain model, this section conducts systematic comparative validation by (a) comparing solution from the equivalent plane-strain model (i.e., Eq. (15)) with those of the ECEM (Eq. (16)), and (b) comparing results from 3D single-drain numerical model are contrasted against its equivalent 2D single-drain counterpart.

By substituting the equivalent permeability coefficient derived from Eq. (23) into Eq. (15), the consolidation degree for the equivalent plane-strain model can be calculated. These results are subsequently compared with the solutions from the ECEM. The relevant parameters used in the comparison are as follows: $b = 100$ mm, $\delta = 4$ mm, $d = 1$ m, $L = 10$ m, $k_h = 10^{-9}$ m/s, $q_w = 100$ m^3/yr, and $\kappa = 3$, $s_{el} = 3$, $m_v = 2.5 \times 10^{-4}$ kPa^{-1}. As illustrated in Fig. 3, the curves of consolidation degree versus time factor for different depths, computed using the equivalent plane-strain model, exhibit excellent agreement with the results from the ECEM. This consistency confirms the validity of the proposed equivalent calculation. Furthermore, the consolidation degree exhibits negligible variation for different depths.

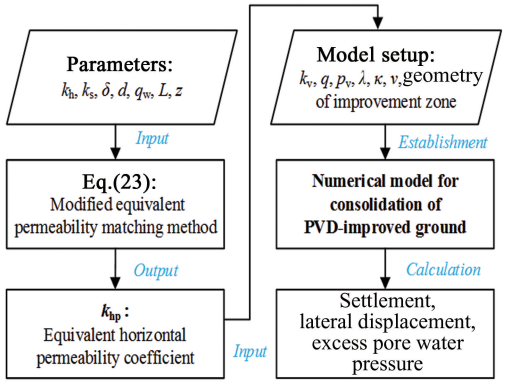

Fig.2 Computational workflow for the modified equivalent plane-strain model of PVDs-improved ground

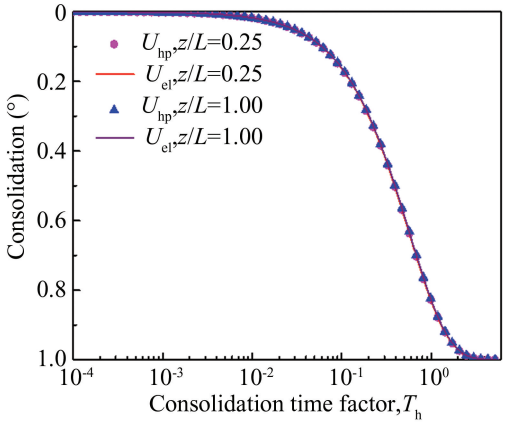

Fig.3 Comparison between ECEM and equivalent plane-strain model in only horizontal drainage

To evaluate the impact of dimensional simplification on computational accuracy, a realistic 3D finite element model (Fig. 4(a)) and an equivalent 2D plane-strain model (Fig. 4(b)) for a single-drain unit are established separately using COMSOL Multiphysics, followed by a comparative analysis on their calculation results. Taking the

following working conditions as an example: PVDs with a cross-sectional dimension of 100 mm × 4 mm are arranged in a square configuration with a spacing of 1 m and an installation depth of 10m; the soil top surface is subjected to an instantaneous surcharge load of 100 kPa, while a vacuum pressure of −80 kPa is applied to the PVDs. Accordingly, the 3D model is defined with geometric dimensions of 1 m × 1 m × 10 m (length × width × height), while in the 2D model, the thickness of equivalent drained wall ($2b_w$) and the thickness of equivalent influence zone ($2B$) are 4 mm and 1 m, respectively. In this comparison, only horizontal seepage is considered, with a horizontal permeability coefficient of 1×10^{-9} m/s. The equivalent horizontal permeability coefficient for the 2D plane-strain model, determined using Eq. (23), is 3.6×10^{-8} m/s. Additional parameters include soil elastic modulus of 4 MPa, porosity of 0.25, density of 2600 kg/m^3, and PVD discharge capacity of 100 m^3/yr. All parameters except the permeability coefficient remain consistent between the 3D and 2D models.

The average excess pore water pressure at mid-depth (z = 5 m) and surface settlement calculated by 3D numerical model, 2D numerical model, and ECEM solution (Eq. (16)), are compared in Figs. 5 and 6. As observed in Fig. 5, the excess pore water pressure calculated by the 3D numerical model aligns almost perfectly with the analytical solution of ECEM (i.e., ECEM solution), confirming that the original model (i.e., ECEM) used in the modified equivalent method effectively accounts for the shape effect of PVDs and accurately simulates the dissipation of the excess pore water pressure. The 2D model slightly underestimates excess pore pressure during the early consolidation stage (during first 10 d) and marginally overestimates it in later stages, though overall differences remain minor. Fig. 6 demonstrates that the ECEM solution closely matches the 3D numerical results for surface settlement. The 2D model initially overpredicts settlement compared to the 3D model but converges to slightly lower values in later stages, with a minimal overall discrepancy.

The above comparative results indicate that the 2D equivalent model offers substantial advantages for numerical modeling, including simplified modeling implementation, reduced computational time, and sufficient accuracy to meet engineering design requirement.

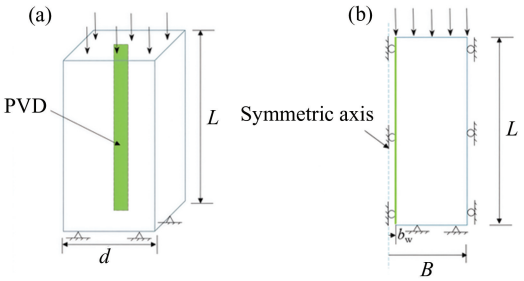

Fig. 4 Geometric schematic diagram of finite element model of single-drain unit: (a) 3D model and (b) 2D equivalent model

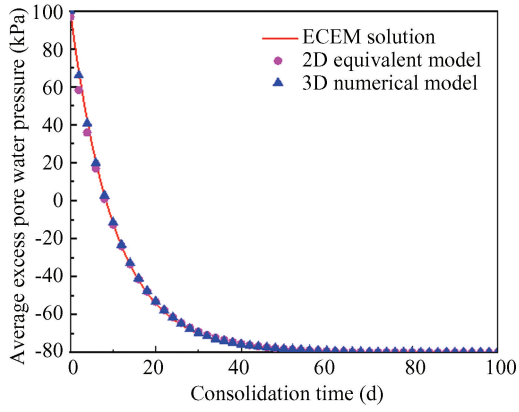

Fig.5 Comparison of excess pore water pressure calculated by 3D numerical model, 2D equivalent plane-strain model, and ECME solution

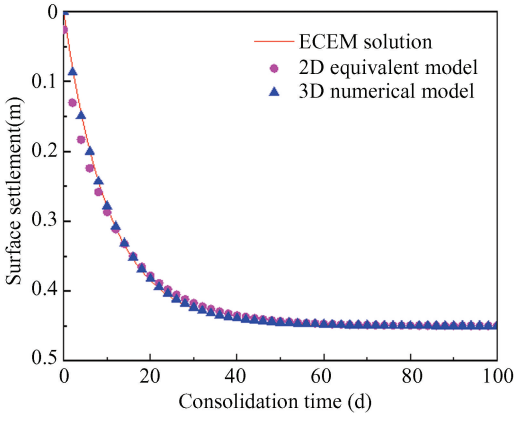

Fig.6 Comparison of surface settlement calculated by 3D numerical model, 2D equivalent plane-strain model, and ECME solution

3 Application to Case History

To further validate the applicability of the proposed modified plane-strain model in analyzing the

consolidation problem of drain-group systems, the field monitoring data of a ground improvement project at Tianjin Port, as reported by Chu et al.[35], are used for validation. Tianjin Port, situated at the estuary of the Haihe River in the Bohai Bay, was constructed on a muddy coastal area where the land was entirely formed through land reclamation. The soil profile at the terminal yard consists of layered deposits: from 0 to 3.5 m depth, silty clay originating from the seabed, with a water content of 20% – 60%, a void ratio of 0.4–1.2, and a shear strength of 20 kPa–40 kPa; from 3.5 to 8.5 m depth, mucky clay, displaying higher water content (40%–60%) and void ratio (0.8–1.6) but lower shear strength (20 kPa–30 kPa); from 8.5 to 16 m depth, soft silty clay, showing reduced water content (20% – 40%) and void ratio (0.4 – 1.2) along with improved shear strength (40 kPa–60 kPa); and from 16 to 20 m depth, stiff silty clay, characterized by the lowest water content (0 – 20%) and void ratio (0.4–0.8) yet the highest shear strength (60 kPa–80 kPa), indicating a dense, well-consolidated stratum with excellent load-bearing capacity.

To achieve the target settlement, a total design load of 140 kPa was required, which is challenging to attain through only conventional surcharge preloading. Thus, combined vacuum and surcharge preloading method was adopted. This involved applying an 80 kPa vacuum pressure alongside staged surcharge loads. The treatment area was divided into three zones (Zone I, II, and III) for phased construction, as illustrated in Fig. 7. PVDs were installed to a depth of 20 m in a square arrangement with 1m spacing, and their specifications summarized in Table 1, where the width and thickness of PVD are 100 mm and 3 mm. A 0.3 m- thick sand cushion and an impermeable sealing membrane were placed over the soil surface. Surcharge loading was applied incrementally to ensure stability, with final fill heights of 2.53 m, 3.5 m, and 2.84 m for Zones I, II, and III, respectively, using silty clay fill material with an average unit weight of 17.1 kN/m^3.

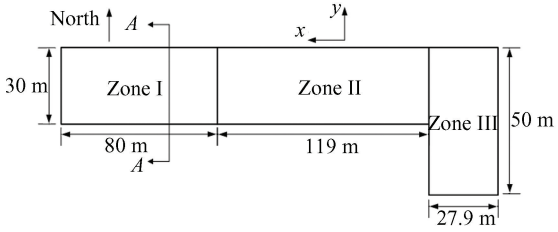

Fig.7 Planning map of Tianjin port ground improvement project

The equivalent horizontal permeability coefficients for each soil layer were computed using the proposed plane-strain equivalence model (Eq. (23)). A 2D equivalent numerical model was subsequently developed in COMSOL Multiphysics. To optimize computational efficiency, the thickness of the equivalent drain wall was simplified to zero, while the smear effect induced by installation disturbance was accounted for by setting $k_h/k_s = 2.5$ and $s_{el} = 4$. Taking Zone I as an example, a north-south cross-section model was constructed, leveraging geometric symmetry to simulate half of the treatment area, as shown in Fig. 8.

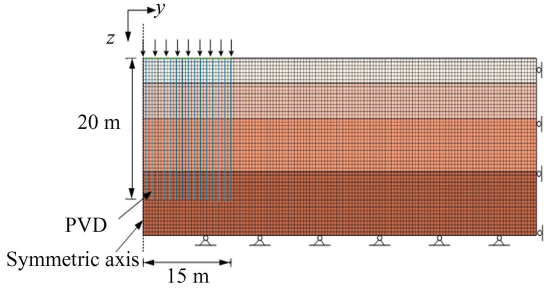

Fig.8 Schematic diagram of 2D numerical model for Zone I

Table 1 PVD parameters

Installation spacing	Setting depth	PVD size	Drainage capacity(qw)
1m	20m	100 mm×3 mm^2	100m^3/yr

The soil was described using the modified Cam Clay constitutive model. In previous numerical studies[36], the modified Cam-clay model has been adopted in both plane-strain and three-dimensional finite element analyses of soft ground improvement involving vertical drains and vacuum preloading. In these analyses[36], consolidation behavior and pore water pressure dissipation were simulated within an effective stress framework, providing a reference basis for the constitutive modeling adopted in the present study. Accordingly, the modified Cam Clay model was employed herein to simulate the consolidation

behavior of soft clay under combined vacuum and surcharge preloading conditions. With material parameters listed in Table 2, full-scale simulation results were obtained through mirroring the computational outputs.

Table 2 Numerical simulation parameters of Tianjin port ground improvement project

Depth (m)	λ	κ	ν	γ (kN/m^3)	k_v (10^{-10}m/s)	k_h (10^{-10}m/s)	k_{hp} (10^{-10}m/s)	OCR
0-3.5	0.12	0.03	0.3	18.3	6.67	20	2.42	1-1.1
3.5-8.5	0.14	0.03	0.25	18.8	13.3	40	4.84	1.2-1.5
8.5-16	0.2	0.04	0.3	17.5	6.67	20	2.42	1.2-1.6
16-20	0.1	0.02	0.27	18.5	1.67	5	0.6	1.1-1.4

Note: λ is compression index of soil, ν is Poisson's ratio of soil, γ is the unit weight of soil, k_v is vertical permeability coefficient of undisturbed soil, OCR is the over-consolidation ratio of the soil.

Fig. 9 shows the contours of excess pore water pressure and soil deformation in Zone I at 10 d, 50 d, and 150 d. Excess pore water pressure dissipates quickly in the areas with PVDs, and by 150 d, the target vacuum pressure of −80 kPa is almost fully attained. At the same time, the vacuum pressure propagates into the two regions without PVDs and the strata beneath the PVDs. The surface settlement decreases radially outward from the surcharge centerline. In the peripheral regions without PVDs, slight settlement occurs, accompanied by pronounced lateral displacement. This indicates that the surrounding soil (without PVDs) exhibits lateral displacement as its primary deformation response to the combined vacuum and surcharge preloading. This characteristics requires special consideration during the design and construction phases. Given this, the next section will delve into the lateral displacement characteristics of the surrounding soil.

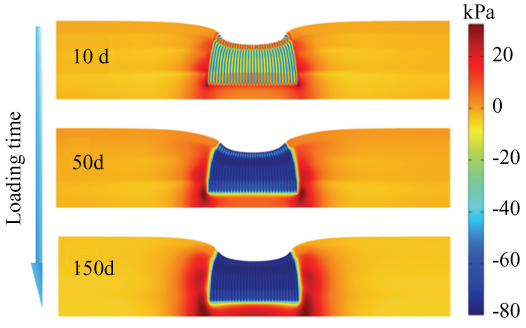

Fig.9 Contours of pore water pressure in Zone I at 10 d, 50 d, and 150 d

Figs.10-12 show comparisons between predicted and measured settlements along the surcharge centerline at different depths. The predictions of numerical model closely match the field measurements, so the model setup and the selected parameters are considered reasonable. In this project, the staged loading sequence was applied. Vacuum pressure was applied first, and surcharge loading was added step by step after the soil gained sufficient strength. Such loading process helps reduce the risk of shear failure because vacuum loading mainly reduces pore water pressure and does not create shear stress in the soil. It can also be found that settlement evolution correlates directly with loading phases: accelerated settlement rates coincide with surcharge increments, while gradual stabilization occurs during constant-load periods. The temporal and spatial agreement between predictions and measurements confirms the capability of the proposed model to capture consolidation behavior induced by PVDs under combined vacuum and surcharge preloading.

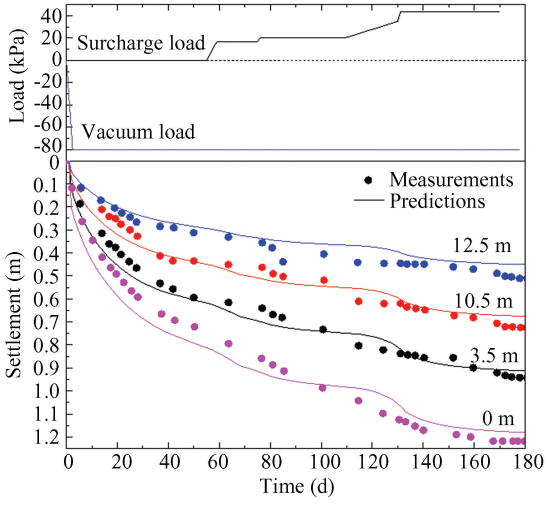

Fig.10 Comparison between predicted and measured settlement for different depths in Zone I

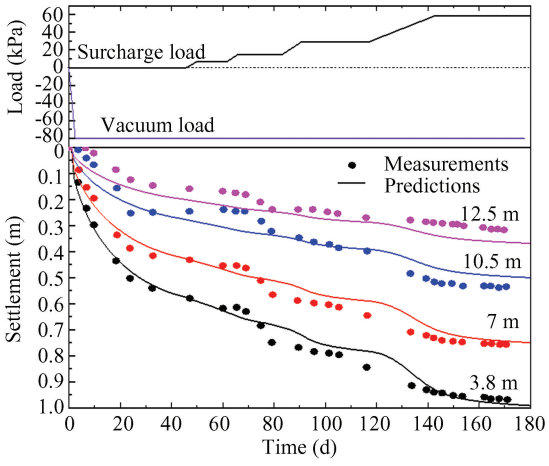

Fig.11 Comparison between predicted and measured settlements for different depths in Zone II

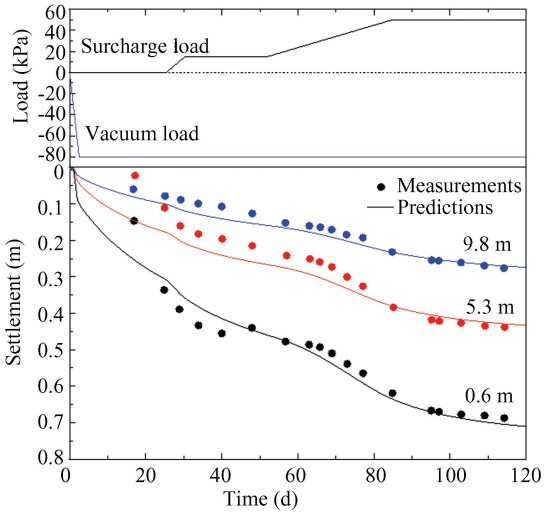

Fig.12 Comparison between predicted and measured settlement for different depths in Zone III

4 Analysis on Lateral Deformation Characteristics of Surrounding Soil

Based on the numerical simulation of Zone I, Figs. 13 and 14 depict distribution patterns of the lateral displacement of surrounding soil along with vertical and horizontal directions, respectively, for different consolidation times. The results indicate that lateral displacements are most pronounced at the soil surface, gradually increasing over time before stabilizing, while diminishing with depth. Additionally, maximum lateral displacements at the soil surface occur near the edges of the treated zone (i.e., preloading zone), and the lateral displacements decrease progressively with distance from the treated zone. Mechanistically, vacuum pressure induces inward lateral deformation (toward the treated zone), whereas surcharge loading generates outward lateral deformation. The deformation rate decreases with increasing effective stress. In this case, however, all observed lateral displacements are negative (directed toward the treated zone). This behavior arises because surcharge loads were applied incrementally after an initial period of vacuum preloading, and the magnitude of surcharge was limited to avoid significant outward deformation.

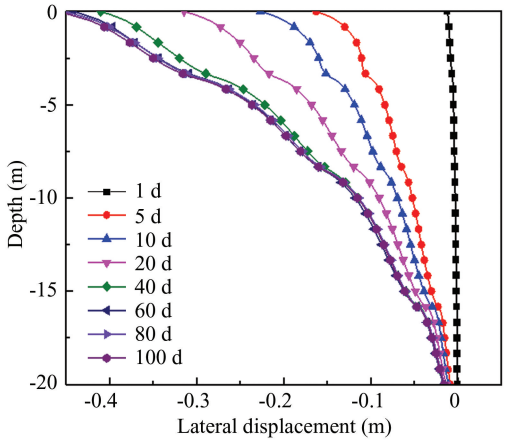

Fig.13 Distribution curves of lateral displacement at 15m from the central axis along depth in Zone I

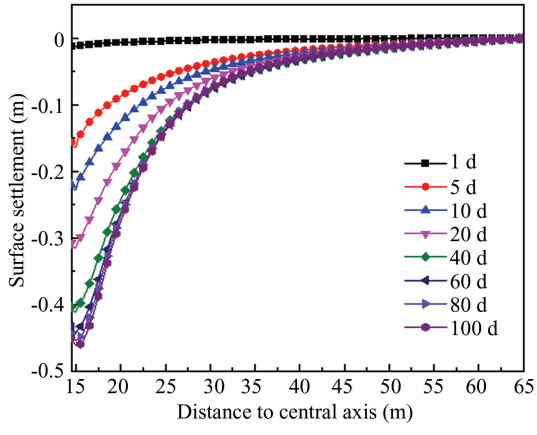

Fig.14 Distribution curves of lateral displacement at soil surface along horizontal direction in Zone I

Building upon the parametric conditions of the aforementioned case study, following investigation examined the influence of varying load combinations and loading rates on lateral deformations, focusing on ramp load commonly encountered in engineering

practice. The analysis evaluated lateral displacement behavior in soils adjacent to the treated zone under different total surcharge magnitudes and loading rates. The loading configurations are illustrated in Fig. 15.

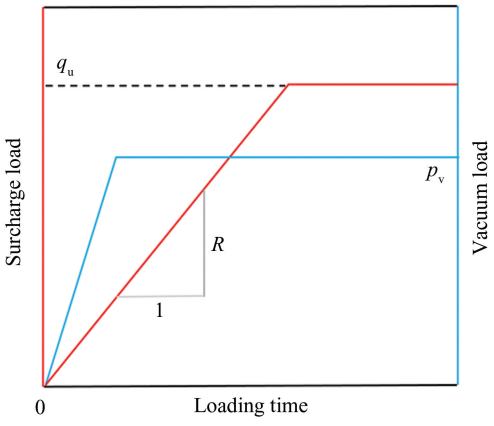

Fig.15 Pattern of ramp combined vacuum and surcharge load

With vacuum pressure fixed at 80 kPa, four surcharge magnitudes (q_u = 40, 60, 80, and 100 kPa) were analyzed. Lateral displacement profiles at the treated zone edge (x=15 m) for 50 d, 100 d, and 150 d are shown in Fig. 16. It can be found that larger surcharge magnitudes amplify outward displacements, particularly in the upper soil layer (0–3.5 m). For $q_u \leqslant 80$ kPa, the lateral displacement in the upper soil layer exhibits depth-dependent directional reversal: inward displacement near the surface transitions to outward displacement at a depth before reverting to inward displacement deeper down. For q_u = 100 kPa, outward displacement dominates throughout the upper layer. Notably, maximum outward displacements occur not at the soil surface but at a shallow subsurface depth, with peak magnitudes consistently localized to similar depth across cases.

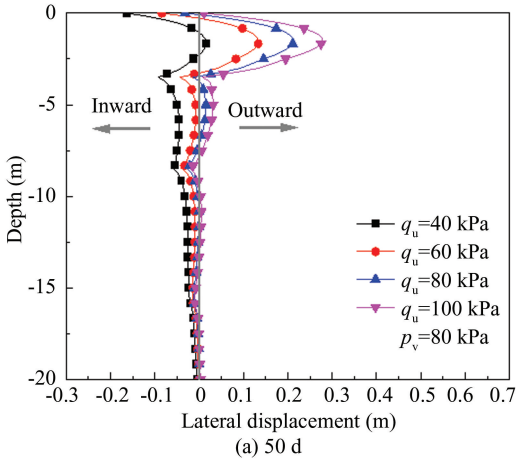

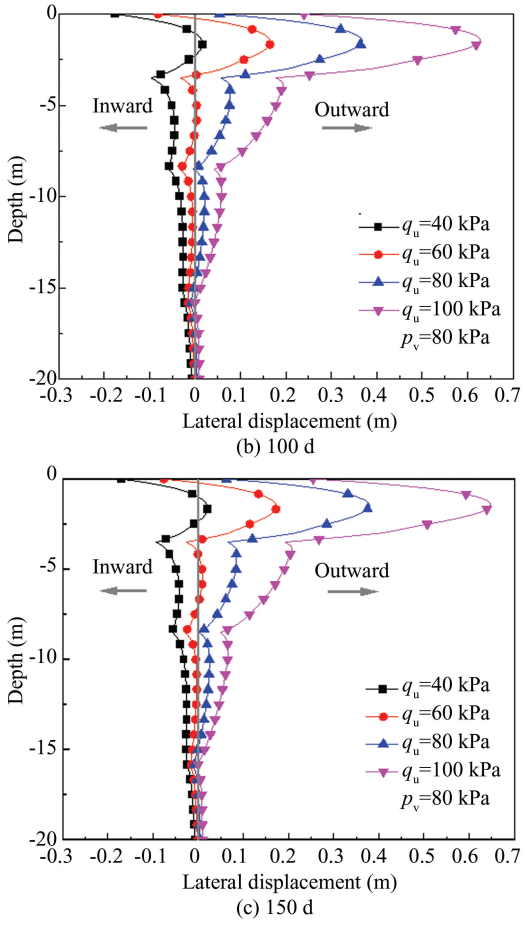

Fig.16 Lateral displacement at treated zone edge under different load combinations

Overall, the lateral displacements attenuate with depth, becoming negligible near the bottom of PVDs. In addition, the outward lateral displacement increases as consolidation progresses. Among the four load combinations, the 60 kPa surcharge combined with 80 kPa vacuum pressure yields minimal overall lateral displacements.

The influence of loading rate was further analyzed under constant vacuum pressure (−80 kPa) and total surcharge (60 kPa). As shown in Fig. 17, higher loading rates increase outward displacements at the treated zone edge despite identical total load magnitudes. The maximum lateral displacements still occur at a depth within the first soil layer rather than at the surface. The loading rate has a greater impact on the lateral displacement of the near-surface soil layer compared to the deeper layers. Mechanistically, the outward lateral displacements are driven by surcharge-induced horizontal expansion, while the inward lateral displacements result from vacuum-induced horizontal contraction.

Under surcharge loading, soil deformation can be attributed to three main mechanisms. First, the soil beneath the surcharge undergoes simultaneous vertical compression and lateral expansion. Second, deformation at the bottom boundary is restrained, and the disturbance induced by the surcharge gradually decreases with depth. Third, the surcharge leads to inward concavity of the soil on both sides of the shallow zone. Under the combined influence of these three mechanisms, the maximum lateral displacement consistently occurs in the shallow layer at a depth of 2 – 3 m and is not affected by the load magnitude or the loading rate, as shown in Figs. 16 and 17.

In practical engineering applications, combined vacuum and surcharge preloading serves as an effective method to mitigate lateral displacements. Based on the aforementioned analysis, minimizing the impact of lateral displacements on the surrounding soil requires an optimal design of combined vacuum and surcharge preloading. When the total load magnitude is fixed, strategic modulation of the loading rate can further reduce lateral deformations.

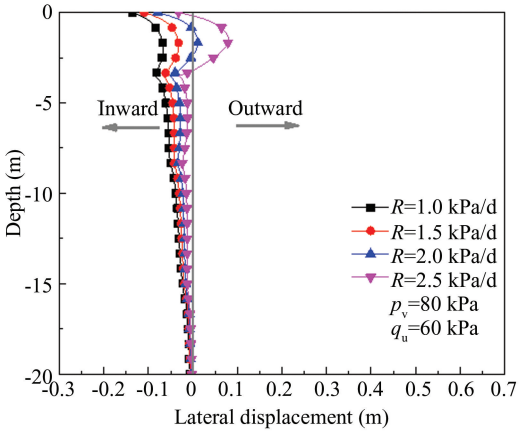

(a) 10 d

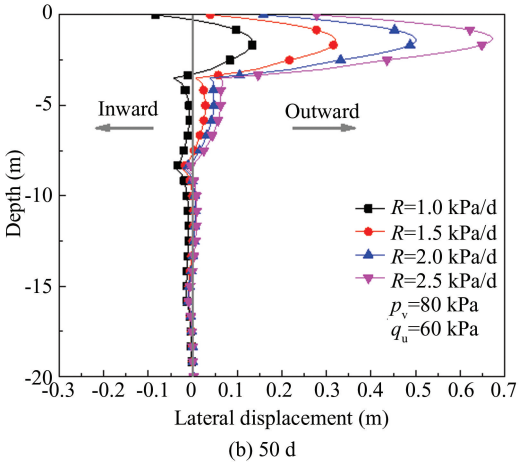

(b) 50 d

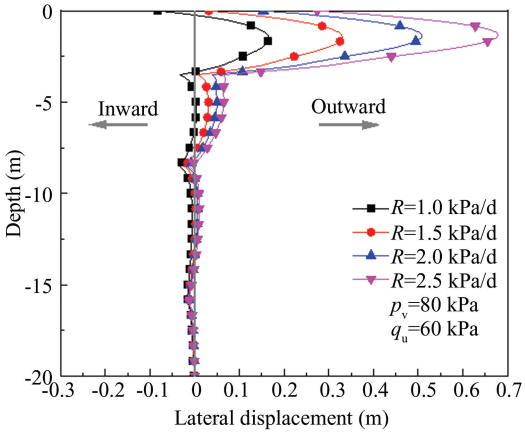

(c) 100 d

Fig.17 Lateral displacement at treated zone edge under different loading rates

5 Conclusions

The modified equivalent plane-strain model for the soft soil improved by PVDs combined with surcharge and vacuum preloading was developed based on the permeability matching method, achieving the consideration of the shape effect of PVDs into numerical simulation. The proposed model was validated by comparing with the analytical solution of ECEM and realistic 3D finite element model. Meanwhile, the applicability of the proposed model for analyzing drain-group ground system was validated through comparison between the predicted settlement from finite element model and measured settlement. Notably, the proposed 2D equivalent model offers a substantial advantage in computational efficiency over full 3D modeling, and by incorporating the shape effect of PVDs, it provides an efficient computational tool for predicting both settlement and lateral deformation in large – scale ground improvement projects. Based on the numerical model, the lateral deformation characteristics of the surrounding zone without PVDs were investigated. The main conclusions can be drawn as follows:

(1) During combined surcharge and vacuum preloading, the treated zone with PVDs installation mainly experiences vertical settlement deformation, while surrounding soils without PVDs predominantly undergo lateral deformation. The most significant lateral displacement occurs near the edge of the treated zone.

(2) Among the load combinations discussed in this paper, an 80 kPa vacuum pressure combined with a 60 kPa surcharge results in the minimal overall lateral displacement. Increasing either the surcharge magnitude or the loading rate amplifies outward displacements. For instance, when the total surcharge magnitude keeps 60 kPa, increasing the loading rate from 1 kPa/d to 2.5 kPa/d results in a 200% increase in the maximum outward displacement by 50 d. The maximum lateral displacement typically occurs at a subsurface depth of 2-3 m, rather than at the surface.

(3) Under the loading conditions (a vacuum pressure of 80 kPa combined with a staged surcharge load) from the analyzed case history, the surrounding soils undergo inward lateral deformations. These lateral displacements exhibit progressive attenuation with increasing vertical depth and/or horizontal distance from the central axis of loading.

(4) In ground improvement projects, combined vacuum and surcharge preloading serves as an effective method for mitigating lateral displacements. When the total applied load remains constant, moderating the loading rate can significantly reduce the influence of lateral displacements on adjacent environments.

References

[1] Liu J J, Luo X S, Lei H Y, et al. Dredged clay treatment consolidation theory by air-booster vacuum preloading. Journal of Geotechnical and Geoenvironmental Engineering, 2024, 150(5): 05024001. DOI: 10.1061/JGGEFK.GTENG-11918.

[2] Ma K, Gao Z Q, Wang J, et al. Nonlinear consolidation finite element analysis of a layered soft soil foundation under multistage loading based on the continuous drainage boundary. Computers and Geotechnics, 2024, 169: 106220. DOI:10.1016/j.compgeo.2024.106220.

[3] Cao Y P, Cui X Z, Qiu Z H, et al. Investigation on dewatering and reinforcement of dredged clay treated with SAP and PVD under vacuum preloading. Geotextiles and Geomembranes, 2025, 53(6): 1407-1422. DOI: 10.1016/j.geotexmem.2025.07.004.

[4] Zhou Y, Bian J, Tao H, et al. Comparison of geotextiles by aeration vacuum rapid dewatering technique on dredged sludge. Journal of Harbin Institute of Technology (New Series), 2016, 23(4): 5. DOI: 10.11916/j.issn.1005-9113.2016.04.004.

[5] Zhang J, Zong M F, Wu W B, et al. Analytical solution for radial consolidation of combined electroosmosis-vacuum-surcharge preloading considering free strain and cyclic loading. Computers and Geotechnics, 2024, 176: 106810. DOI:10.1016/j.compgeo.2024.106810.

[6] Xu F, Yang J F, Wu Q C, et al. Prediction method for lateral deformation of PVD-improved ground under vacuum preloading. Geotextiles and Geomembranes, 2025, 53(4): 1021-1034. DOI:10.1016/j.geotexmem.2025.03.008.

[7] Ni J J, Liu S S, Wang Y C, et al. Synergistic influence of lime and straw on dredged sludge reinforcement under vacuum preloading. Construction and Building Materials, 2024, 421: 135642. DOI: 10.1016/j.conbuildmat.2024.135642.

[8] Tian Y, Jiang G S, Wu W B, et al. Elliptical cylindrical equivalent model of PVD-assisted consolidation under surcharge combined with vacuum preloading and its application. Computers and Geotechnics, 2021, 139: 104389. DOI: 10.1016/j.compgeo.2021.104389.

[9] Anda R, Chai J C, Negami T. Effect of chemical additives on the consolidation behaviours of mini-PVD unit cells-from macro to micro. Geotextiles and Geomembranes, 2023, 51(1): 199-208. DOI: 10.1016/j.geotexmem.2022.10.008.

[10] Wu W B, Wang Z Q, Zhang Y P, et al. Semi-analytical solution for negative skin friction development on deep foundations in coastal reclamation areas. International Journal of Mechanical Sciences, 2023, 241: 107981. DOI: 10.1016/j.ijmecsci.2022.107981.

[11] He Z L, Sun H L, Chu J, et al. Image-based deformation characterization of dredged soil during consolidation under vacuum preloading with horizontal drains. Journal of Geotechnical and Geoenvironmental Engineering, 2025, 151(7): 04025058. DOI: 10.1061/JGGEFK.GTENG-13077.

[12] Zhang L, Jin H H, Lv Y D, et al. Improvements in vacuum-surcharge preloading combined with electro-osmotic consolidation on soft clayey soil with high water content. Geotextiles and Geomembranes, 2025, 53(1): 41-54. DOI:10.1016/j.geotexmem.2024.09.004.

[13] Yin J H, Chen W B, Wu P C, et al. Field study of a sustainable land reclamation approach using dredged marine sediment improved by horizontal drains under vacuum preloading. Journal of Geotechnical and Geoenvironmental Engineering, 2024, 150(11): 04024114. DOI: 10.1061/JGGEFK.GTENG-12632.

[14] Wu Y, Wu J J, Lu Y T, et al. Experimental study on vacuum preloading combined with intermittent airbag pressurization for treating dredged sludge. Geotextiles and Geomembranes, 2025, 53(1): 366-377. DOI: 10.1016/j.geotexmem.2024.11.001.

[15] Xu F, Peng Y F, Lu Y T, et al. Modified method for predicting lateral displacement of PVD-improved ground under combined vacuum and surcharge loading. Geotextiles and Geomembranes, 2023, 51(4): 173-187. DOI: 10.1016/j.geotexmem.2023.04.003.

[16] Reginald A, Barron J A, et al. Consolidation of fine-grained soils by drain wells by drain wells. Transactions of the American Society of Civil Engineers, 1948, 113(1): 718-742. DOI:10.1061/TACEAT.0006098.

[17] Zhou W H, Lok T M H, Zhao L S, et al. Analytical solutions to the axisymmetric consolidation of a multi-layer soil system under surcharge combined with vacuum preloading. Geotextiles and Geomembranes, 2017, 45(5): 487-498. DOI: 10.1016/j.geotexmem.2017.06.003.

[18] Zhu G F, Yin J H. Consolidation analysis of soil with vertical and horizontal drainage under ramp loading considering smear effects. Geotextiles and Geomembranes, 2004, 22(1-2): 63-74. DOI: 10.1016/S0266-1144(03)00052-9.

[19] Lu M M, Xie K H, Wang S Y. Consolidation of vertical drain with depth-varying stress induced by multi-stage loading. Computers and Geotechnics, 2011, 38(8): 1096-1101. DOI: 10.1016/j.compgeo.2011.06.007.

[20] Lu M M, Li D X, Jing H W, et al. Analytical solution for consolidation of band-shaped drain based on an equivalent annular drain. International Journal of Geomechanics, 2019, 19(6): 04019043. DOI: 10.1061/(ASCE)GM.1943-5622.0001423.

[21] Hansbo S. Consolidation of clay by band-shaped prefabricated drains. Ground Engineering, 1979, 12(5): 16-25.

[22] Fellenius B H, Castonguay N G. The efficiency of band shaped drains: A full scale laboratory study. Report to National Research Council and the Industrial Research Assistance Programme, Ottawa, 1985, 54.

[23] Pradhan T. B. S, Imai G, Murata T, et al. Experimental study on the equivalent diameter of a prefabricated band-shaped drains. Proceedings of Eleventh Southeast Asian Geotechnical Conference. Singapore: SEAGC, 1993, 391-396. https://cir.nii.ac.jp/crid/1573387448944836864.

[24] Long R P, Covo A. Equivalent diameter of vertical drains with an oblong cross section. Journal of Geotechnical Engineering, 1994, 120(9): 1625-1630. DOI: 10.1061/(ASCE)0733-9410(1994)120:9(1625).

[25] Abuel-Naga H, Bouazza A. Equivalent diameter of a prefabricated vertical drain. Geotextiles and Geomembranes, 2009, 27(3): 227-231. DOI: 10.1016/j.geotexmem.2008.11.006.

[26] Huang C X, Deng Y B, Chen F. Consolidation theory for prefabricated vertical drains with elliptic cylindrical assumption. Computers and Geotechnics, 2016, 77: 156-166. DOI: 10.1016/j.compgeo.2016.04.015.

[27] Tian Y, Wu W B, Jiang G S, et al. Analytical solutions for vacuum preloading consolidation with prefabricated vertical drain based on elliptical cylinder model. Computers and Geotechnics, 2019, 116: 103202. DOI: 10.1016/j.compgeo.2019.103202.

[28] Tian Y, Wu W B, Wen M J, et al. Nonlinear consolidation of soft foundation improved by prefabricated vertical drains based on elliptical cylindrical equivalent model. International Journal for Numerical and Analytical Methods in Geomechanics, 2021, 45(13): 1949-1971. DOI: 10.1002/nag.3250.

[29] Tian Y, Jiang G S, Wu W B, et al. Elliptical cylindrical equivalent model for consolidation of unsaturated soil improved by PVD. International Journal for Numerical and Analytical Methods in Geomechanics, 2022, 46(17): 3123-3153. DOI: 10.1002/nag.3443.

[30] Tian Y, Wu W B, Wang P, et al. Large-strain consolidation of PVD-improved soils considering depth-dependent initial void ratio and initial effective stress due to soil self-weight. International Journal for Numerical and Analytical Methods in Geomechanics, 2023, 47(15): 2791-2814. DOI: 10.1002/nag.3598.

[31] Lu Y T, Chai J C, Ding W Q. Predicting deformation of PVD improved deposit under vacuum and surcharge loads. Geotextiles and Geomembranes, 2020, 48(1): 32-40. DOI: 10.1016/j.geotexmem.2019.103502.

[32] Hird C C, Pyrah I C, Russel D. Finite element modelling of vertical drains beneath embankments on soft ground. Geotechnique, 1992, 42(3): 499-511. DOI: 10.1680/geot.1992.42.3.499.

[33] Hird C C, Pyrah I C, Russel D, et al. Modelling the effect of vertical drains in two-dimensional finite element analyses of embankments on soft ground. Canadian Geotechnical Journal, 1995, 32(5): 795-807. DOI: 10.1139/t95-07.

[34] Indraratna B, Redana I W. Plane-strain modeling of smear effects associated with vertical drains. Journal of Geotechnical and Geoenvironmental Engineering, 1997, 123(5): 474-478. DOI: 10.1061/(ASCE)1090-0241(1997)123:5(474).

[35] Chu J, Yan S W. Estimation of degree of consolidation for vacuum preloading projects. International Journal of Geomechanics, 2005, 5(2): 158-165. DOI: 10.1061/(ASCE)1532-3641(2005)5:2(158).

[36] Indraratna B, Rujikiatkamjorn C, Balasubramaniam A S, et al. Soft ground improvement via vertical drains and vacuum assisted preloading. Geotextiles and Geomembranes, 2012, 30: 16-23. DOI: 10.1016/j.geotexmem.2011.01.004.